Journal of
Micro/Nanolithography,
MEMS, and MOEMS

Nanolithography.SPIEDigitalLibrary.org

In-chip direct laser writing of a centimeter-scale acoustic micromixer

Jorick van 't Oever
Niels Spannenburg
Herman Offerhaus
Dirk van den Ende
Jennifer Herek
Frieder Mugele

SPIE.

In-chip direct laser writing of a centimeter-scale acoustic micromixer

Jorick van 't Oever,[a,b,*] Niels Spannenburg,[a] Herman Offerhaus,[a] Dirk van den Ende,[b] Jennifer Herek,[a] and Frieder Mugele[b]
[a]University of Twente, Optical Sciences, P.O. Box 217, 7500 AE, Enschede, The Netherlands
[b]University of Twente, Physics of Complex Fluids, P.O. Box 217, 7500 AE Enschede, The Netherlands

Abstract. A centimeter-scale micromixer was fabricated by two-photon polymerization inside a closed microchannel using direct laser writing. The structure consists of a repeating pattern of 20 μm × 20 μm × 155 μm acrylate pillars and extends over 1.2 cm. Using external ultrasonic actuation, the micropillars locally induce streaming with flow speeds of 30 μm s^{-1}. The fabrication method allows for large flexibility and more complex designs. [DOI: 10.1117/1.JMM.14.2.023503]

Keywords: microfabrication; direct laser writing; microfluidics; ultrasonic streaming; confocal laser scanning microscopy.

Paper 14169 received Dec. 18, 2014; accepted for publication Apr. 1, 2015; published online Apr. 21, 2015.

1 Introduction

Over the last decade, there has been a considerable development in the field of mixing in microfluidic devices.[1–3] Mixing, passive or active, is part of many laboratory methods, therefore, adapting it to the microscale and nanoscale is important for lab-on-a-chip and microscale total analysis systems.[4] Fluidics at this scale are typically dominated by viscous forces and turbulent mixing this is hard to achieve.

One class of active mixers is ultrasonic mixers, which use acoustic fields at ultrasonic frequencies. Typically, these mixers either excite a flow at the sidewalls of a microfluidic chamber[5–7] or excite a flow inside the chamber using a bubble.[8–10] In the case of homogeneous mixing, the chamber size is limited by the spatial extent of the induced flows, which subsequently limits the flow rate. Bubbles can be placed inside the volume and allow higher throughput compared with sidewall induced flows, enabling fast mixing.[11] However, bubble-based micromixers also show serious challenges[7,12] with regard to stability. The excitation frequency must closely match the geometric resonance frequency,[13] therefore, it is dependent on flow rate[11] and is influenced by contamination and dissolving over time.

The mixer shown in this paper operates by locally exciting flow around pillars embedded inside the microchannel, providing the main advantage of bubble-based mixing without the mentioned drawbacks. This method allows, in principle, for a larger channel cross section and effective mixing dispersed over that cross section, enabling high flow rates combined with improved stability compared with bubble mixers. To compensate for lower induced mixing flow speed, many micropillars in a row are used. In this paper, we explore the use of in-chip direct laser writing (DLW) as a fabrication technique for the mixing structure, which requires accurate and repeatable pillar placement and shape over an extensive distance.

*Address all correspondence to: Jorick van 't Oever, E-mail: j.j.f.vantoever@utwente.nl

DLW is a flexible fabrication method for small batches of arbitrarily shaped microstructures. Using two-photon polymerization, only the resist in the focal volume is cured. By displacing the focus with respect to the substrate arbitrarily shaped three-dimensional (3-D) structures can be created. The height of the freestanding structures is limited by their structural strength.

The maximum fabricated size in previously reported work is limited to hundreds of micrometers.[14,15] In this work, we explore a strategy for in-chip DLW fabrication of microstructures on a centimeter scale. An important aspect in this work is the choice of resist, enabling a faster and simpler workflow.[15] The resist has a low viscosity, making it suitable for straightforward filling, development, and cleaning by flowing chemicals directly through the microsystem. The resist also does not require preexposure or postexposure baking. This, combined with the improved handling, enables a 10× faster preparation and development process (2.5 h versus 26 h) compared to earlier methods.[16] Confocal laser scanning microscopy (CLSM) is used to nondestructively characterize the in-chip fabricated structures.[17] As opposed to scanning electron microscopy, CLSM only requires optical access to the sample. Previously, DLW has been used to fabricate a wide variety of structures, such as nanochannels,[18] "overpass"-structures for microfluidics,[19] gold substrates for surface enhanced Raman scattering[20] (SERS), and nanoshells.[21]

Integration into larger structures, as those needed for microfluidics,[22] is not straightforward. Due to the difference in scale, DLW cannot easily be used to fabricate both the structures and the channels since that would take an unacceptably long time. As such microstructures fabricated by DLW are usually fabricated separately from the channels, requiring fine control of structure size during fabrication and accurate alignment during assembly. The same is true for strategies where the structure is partially embedded into a channel which is subsequently covered with a glass or polydimethylsiloxane layer.[23] Examples of other in-chip fabrication techniques are 3-D patterning using laminar flows,[24] patterning of surfaces using microchannel networks,[25] and

structured elastomeric membranes.[17] However, these techniques do not offer the flexibility of arbitrary shapes as is the case with DLW.

In-chip DLW enables the direct integration of various functional structures into existing microchannels. Resist is flowed into the existing channels and structures are directly written and anchored into place. This ensures a good fit and reduces the amount of chemicals required. In-chip DLW was first used for enzymatic 3-D microreactors by Iosin et al.[26] Amato et al.[16] fabricated a porous filter into an existing microchannel and Serra et al.[14] fabricated nematic liquid crystal cells. Wu et al.[27] demonstrated fabrication of both channels and microstructures by combined DLW and direct femtosecond-laser writing.

DLW allows rapid prototyping of 3-D microstructures without the need for masks for each variation. The work presented in this paper provides the basis for more complicated structures, including structures which require full 3-D capability fabricated with DLW with an extensive length. At the same time, in-chip DLW provides good bonding of structures which is important for the robustness of the micromixer and mitigates the problem of alignment during assembly. In the next section, we will first explain the in-chip DLW fabrication process, after which we characterize the structure in terms of geometry and strength. We show the limits of this fabrication method for long microstructures and finally we show acoustic mixing around the micropillars.

2 Experimental Methods

2.1 *Fabrication*

The DLW system (Photonic Professional, Nanoscribe) uses a femtosecond pulsed laser at a 780-nm wavelength and an 80 MHz repetition rate. The system contains a Zeiss Axiovert inverted microscope with an autofocus/interface finding system and charge-coupled device (CCD) camera. The sample is moved using a positioning system consisting of a motorized stage and piezo stage. The motorized stage is used for coarse movements and has a lateral range of 100 mm in both directions and a position accuracy better than 1 μm. The piezo stage is used for the laser writing and has a range of 300 μm $\times$ 300 μm $\times$ 300 μm.

An objective with a higher numerical aperture (NA) produces a smaller focal spot and higher resolution but also produces a smaller polymerized volume. For writing large structures, a lower NA objective and increased laser power reduce writing time at the expense of resolution. However, the aspect ratio of the focal volume scales inversely with the NA, so that a lower NA translates into a more elongated focal volume. For in-chip laser writing the objective working distance is also important, as this limits the maximum axial size of the structures.

The objective we used is a Zeiss LD Plan-Neofluar 63× with an NA of 0.75 and a working distance of 1.7 mm, resulting in lateral and axial DLW resolutions of 560 nm and 5.5 μm, respectively. The resist is a negative tone acrylate-based resist (IP-L, Nanoscribe). IP-L does not require prebaking or postbaking and has a low viscosity (0.8 Pa s) such that direct injection into microchannels is possible.

The microchannel used for in-chip DLW was fabricated using photolithography and deep reactive-ion etching on a ⟨100⟩ silicon wafer. Access holes of 1-mm diameter were made from the backside in the same way as the channels. The channel wafer is anodically bonded to a 500-μm thick borofloat glass wafer and then diced into glass-silicon microchannel chips measuring 6 $\times$ 1.5 cm (see Fig. 1). The length L_c, width w_c, and depth h of the microchannel are 4 cm, 373 μm, and 155 μm, respectively.

The microchannel is filled with resist by connecting a tube to one of the access holes and manually filling the channel using a syringe. The tube is then removed and the chip is placed glass-down into the sample holder in the DLW system.

Sample tilt and rotation correction are performed using the interface finder and CCD. The writing of structures is performed from the silicon toward the glass (see Fig. 2) to prevent an aberrated structure due to diffraction from previously polymerized resist.

Large structures are written in sections using the piezo stage, then the motorized stage is used to move the sample to the beginning of the next section.

After writing, the sample is removed from the sample holder and tube connectors are connected to the access holes. Using a syringe pump (PHD 4400, Harvard Apparatus), first 20 mL propylene glycol monomethyl ether acetate (RER600, Fujifilm) developer is flowed through the channel at a flow rate of 20 mL h^{-1}, followed by 20 mL isopropanol at 20 mL h^{-1}. A gentle flow of air is applied over the access holes until all isopropanol has evaporated, which take less than 30 s.

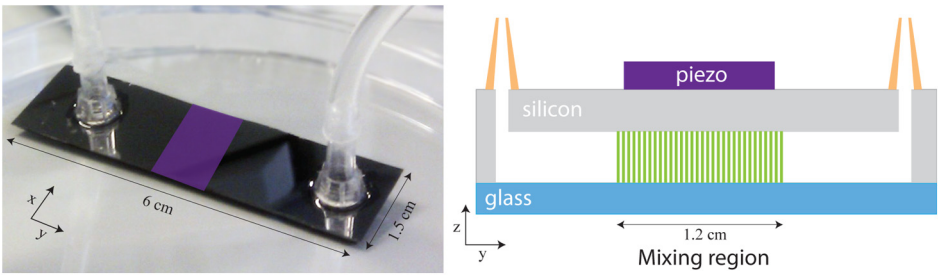

Fig. 1 (a) Photograph and (b) cross-sectional sketch of the mixing device (not to scale). The chip consists of a microchannel etched into silicon (gray), sealed with borofloat glass (blue). Access holes are etched into the backside of the chip on which tubing is connected (orange). The mixing structure fabricated using direct laser writing (green) consists of two parallel rows of square pillars, both rows extending over a region of 1.2 cm. The acoustic mixing is excited using a piezo-element which is placed on top of the chip (illustrated in purple in both photograph and sketch). See Fig. 2 for a cross-sectional sketch in the xz-direction.

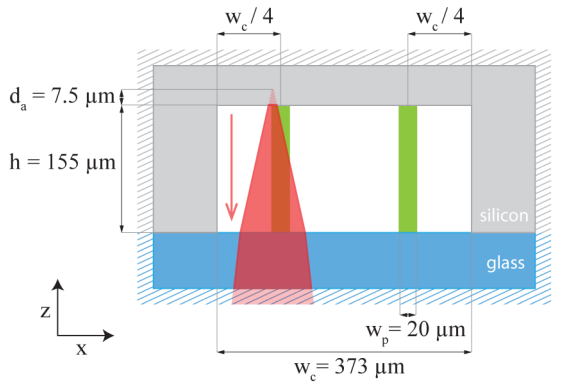

Fig. 2 A cross-sectional sketch of the microchannel with the designed structure. The chip consists of a microchannel with width $w_c = 373\ \mu$m and height $h = 155\ \mu$m. The structure (green) consists of two rows of square pillars, each extending over the full height of the channel and having a width of $w_p = 20\ \mu$m. The rows are placed at a quarter and three quarters of the channel width. Each pillar is written using the focused laser beam (red) with the starting position of the focus designed to be at an anchoring depth $d_a = 7.5\ \mu$m inside the silicon. The progression of writing is from the silicon toward the glass as indicated by the arrow.

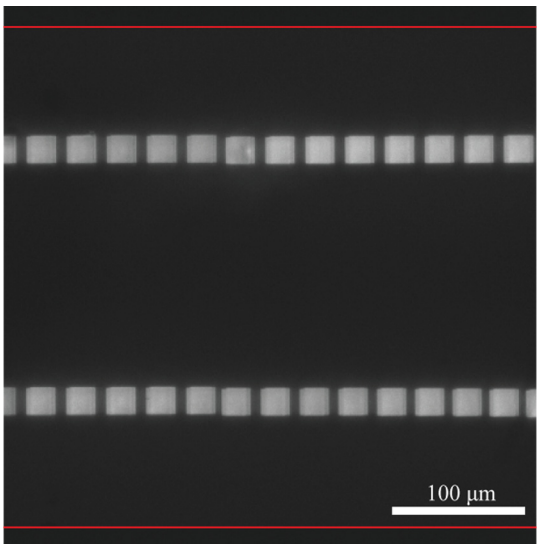

Fig. 3 Fluorescence image of part of the double row structure with $\Lambda = 30\ \mu$m. Visible are four consecutively written pillar sections, with small jumps between sections by the motorized stage visible. The lines (red) indicate the microchannel walls.

2.2 *Characterization*

2.2.1 *Structural analysis*

For the 3-D analysis of the structures, we use CLSM. The channel is filled with index matching oil (Nikon immersion oil, $n = 1.5$) to limit image deterioration by diffraction. We use a home-built CLSM based on a Nikon TE300 inverted microscope, with a 25 mW, 488-nm laser (iFlex-Mustang 488, QiOptiq), spinning disk-based confocal scanner (Ultra View ERS, Perkin Elmer), and camera (C4742-95-12ERG, Hamamatsu). The axial z-position of the objective (S Plan Fluor ELWD 60X NA 0.7, Nikon) was scanned using an objective piezo scanner (PIFOC P-720, Physik Instrumente) with a range of 100 μm. Only the emitted autofluorescence from the structure was transmitted to the camera using a low-pass emission filter with a cut-off wavelength of 525 nm. For the overview image in Fig. 3, a regular fluorescence microscope (TE2000, Nikon) was used with a lower magnification objective (S Plan Fluor ELWD 45X NA 0.45, Nikon). An autofluorescence excitation-emission map of the cured polymer can be found in the Appendix.

2.2.2 *Acoustic mixing*

To visualize the acoustic mixing, we use the same CLSM. The channel is filled with glycerol water mixture (80:20 ratio by weight), in which an 18% volume fraction of fluorescent silica tracer particles is suspended. The mixture is index matched to the silica particles. The spheres have an outer diameter of $2r = 1\ \mu$m and a core of 0.5-μm diameter filled with fluorescein isothiocyanate fluorophore. The fundamental acoustic resonance of the channel at $f = 1.92$ MHz, corresponding to a standing wave along the channel width, is excited using a piezo plate (PZ 26-302, Ferroperm) connected to an amplifier and function generator. The piezo plate is attached on top of the chip using a drop of paraffin oil as the coupling liquid.

Assuming a plane wave resonance, the magnitudes of the acoustic radiation force and the Stokes drag are[28]

$$F_{\text{rad}} = 4\pi\Phi k r^3 E_{\text{ac}} \sin(2kx), \tag{1}$$

$$\Phi = \frac{1}{3}\left[\frac{5\frac{\rho_p}{\rho_m} - 2}{2\frac{\rho_p}{\rho_m} + 1} - \frac{k_p}{k_m}\right], \tag{2}$$

$$k = \frac{2\pi f}{c_m} = 2\pi f\sqrt{\rho_m k_m}, \tag{3}$$

$$F_{\text{drag}} = 6\pi\eta r v_p, \tag{4}$$

where Φ is the acoustic contrast factor, E_{ac} is the acoustic energy density, k is the wavenumber of the sound wave, x is the position along the width of the channel, c_m is the speed of sound in the mixture, $\rho_p = 2648\ \text{kg m}^{-3}$ and $\rho_m = 1208\ \text{kg m}^{-3}$ are the densities of the particles and the mixture, $k_p = 280\ \text{TPa}^{-1}$ and $k_m = 255\ \text{TPa}^{-1}$ are the respective compressibilities, $\eta = 60$ mPa s is the viscosity of the mixture, and v_p is the particle speed (values from Refs. 29 and 30). Using $E_{\text{ac}} = 100\ \text{J/m}^3$, a particle speed of $30\ \mu\text{m s}^{-1}$, and evaluating the radiation force at its peak position $x = w_c/4$ gives a ratio of forces $F_{\text{drag}}/F_{\text{rad}} \approx 85$. Therefore, the silica particles are small enough to be used as tracers since the acoustic radiation force is negligible compared with the Stokes drag.

3 Results and Discussion

3.1 *Fabrication*

The micromixer consists of two parallel rows of pillars placed at one quarter and at three quarters of the channel width (see Fig. 2). Each pillar has a designed square cross section of $20\ \mu\text{m} \times 20\ \mu$m and extends over the full depth of the channel. The writing volume extends into the glass and silicon by 7.5 μm, ensuring proper anchoring. Two versions of the structure have been fabricated using different center-to-center spacings (Λ). The first version with

$\Lambda_1 = 30$ μm is used for characterization, the second version with $\Lambda_2 = 70$ μm is used for the acoustic mixing. Both structures have a total length of 1.2 cm.

We used a distance between written lines and planes of 400 nm and 2 μm, respectively, writing at a speed of 1 mm s^{-1} parallel with the channel. Writing is started at an anchoring depth of approximately 7.5 μm into the silicon. The rows are written using the piezo stage in sections of nine subsequent pillars for Λ_1 and four subsequent pillars for Λ_2, alternating between the top and bottom rows after each section and moving to the next section using the motorized stage. Writing time per pillar is 295 s and the total time is approximately 66 and 29 h for Λ_1 and Λ_2, respectively. The average power at the sample is estimated to be 70 mW.

3.2 *Characterization*

The confocal measurements for the structural analysis were done using steps of 100 μm in the z-direction using the objective scanner, 100 ms integration time per slice, and 25 mW of laser power.

With exception of the last 1.1 mm, the fabricated structure closely matches the design with some minor deviations which are discussed in the below sections. The last segment shows strong irregularities, which will be investigated in Sec. 3.2.4.

3.2.1 *Pillar placement*

A typical section is shown in Fig. 3. The average side-to-wall distance between the top row and nearest wall is 84.0 μm and for the bottom row this distance is 81.2 μm. The designed value is 82.3 μm, so the structure is offset from the center of the channel by approximately 2 μm. The average angle between the rows and the walls is 6 mdeg. Corrected for the angle, the standard deviation in distance to the wall is 1.4 μm, which can be explained by the accuracy of the motorized stage. Within rows of nine consecutively written pillars (i.e., for structures written without the use of the motorized stage), the standard deviation in side-to-wall distance is on average 0.3 μm reflecting the accuracy of the piezo stage using a relatively high writing speed.

The horizontal placement of the pillars is less accurate, reflecting an average side-to-side separation of 7.1 ± 1.1 μm. Again, between consecutively written pillars, the variation is smaller with 0.8 μm. The significant deviation from the designed separation of 10 μm is mostly explained by the consistently wider pillars, leaving less space in between. The variation in the width is 0.7 μm, explaining most of the variation between consecutively written pillars. The additional variation is caused by the motorized stage, but also by the writing direction: because of the relatively high speed, the piezo positioning in this direction is less accurate.

3.2.2 *Pillar shapes and cross sections*

At the glass-pillar interface, the pillars have an average width in direction parallel to the channel of 22.5 ± 0.7 μm and a width normal to the channel of 21.5 ± 0.6 μm. The pillars are not perfectly square and are also slightly larger than the designed value of 20 μm. In both the parallel and normal directions, most of the extra width is due to nonzero lateral size of the DLW focal volume. In the parallel direction, additional width comes from the fact that this is the laser writing direction. Given the small variations in the width, both effects could be corrected for in the design.

All pillars extend over the full depth of the channel. The change in cross section over the full height is less than 3 μm in both widths compared with the values at the glass interface. The displacement with respect to the glass surface is less than 4 μm, meaning that the sidewall angle of the pillars is less than 1.5 deg.

3.2.3 *Structural strength*

The fabricated pillars are sufficiently strong for microfluidic applications, such as an ultrasonic micromixer. Forces due to developer and solvent flow, interfacial tension due to evaporation of the solvent and the force due to the ultrasonic pressure resonance have no influence on the structure.

The Reynolds number for the flow is

$$\mathrm{Re} = \frac{\rho \cdot \bar{v} \cdot D_H}{\mu}, \tag{5}$$

where ρ is the density, μ is the dynamic viscosity of the fluid, $\bar{v}$ is the average flow speed, and D_H is the hydraulic diameter. For our case of a completely filled channel with rectangular cross section, D_H equals $2h \cdot w/(h + w)$. The average flow speed is the flow rate divided by the cross section and equals 97 mm s^{-1}. The Reynolds number for the developer and solvent flows is 1.7 and 0.8, respectively, which sufficiently low to treat the flows as laminar.

Due to the presence of the walls, the drag on a single cylinder F_D does not depend on the Reynolds number, but on geometry only and has to be calculated using a wall correction factor $\lambda = F_D/(\mu \cdot v_{\max})$, with $v_{\max}$ the maximum flow speed in the channel.[31,32] For a single circular cylinder in our geometry, $\lambda \approx 4$ and the drag force is estimated to be $F_D = 1$ mN.[33] Estimation of the drag via shear stresses, using a laminar flow profile and no-slip yields the same order of magnitude. Comparing this estimation with our case of square cylinders placed in a row shows that this value should be taken as a lower estimate, since both a square cross section as placing pillars closely in a row increase the drag compared a single round cylinder.[34,35]

Based on the curvatures of the solvent surface surrounding the pillars during evaporation, we estimate a maximum Laplace pressure of -0.8 kPa inside the solvent, corresponding with a peak inward faced capillary force on the outermost pillar of approximately 3 μN.

3.2.4 *Fabrication defects*

The last segment of the structure covers the last 1.1 mm of the double row structure. Here, the structure shows strong deviations from the designed characteristics, potentially limiting the scale on which we can use in-chip DLW.

Some pillars are misplaced toward neighboring pillars, sometimes even touching completely. Toward the end of the section, some pillars are missing, implying that the flow forces during development were potentially the cause. CLSM measurements of pillars close to the beginning of the second segment are shown in Figs. 4 and 5.

Figure 4 shows the cross section of three pillars at 128 μm from the glass interface. The cross sections of the pillars are intact, showing that pillars extend at least to this depth. The left pillar is wider in the direction parallel to the channel than

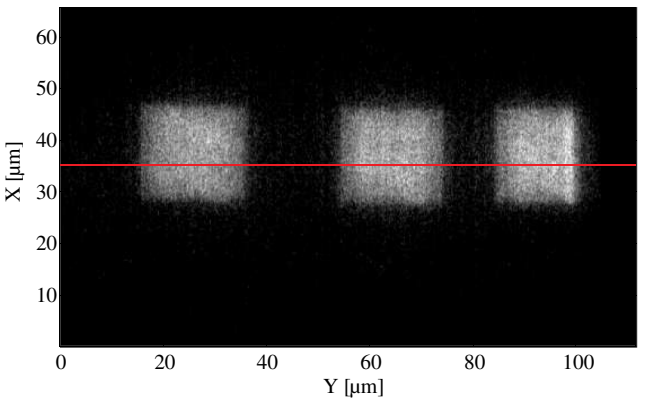

Fig. 4 Cross section of three pillars by confocal laser scanning microscopy (CLSM) taken at 128 μm from the glass interface, as indicated by the line in Fig. 5.

expected, suggesting that the pillar is bent. The side-to-side distance between the first pillar and second is around 16 and is 8.5 μm between the second and third, again indicating a writing error or bending in the first pillar. The right pillar is cut-off due to optical reflections and seems narrower than in reality.

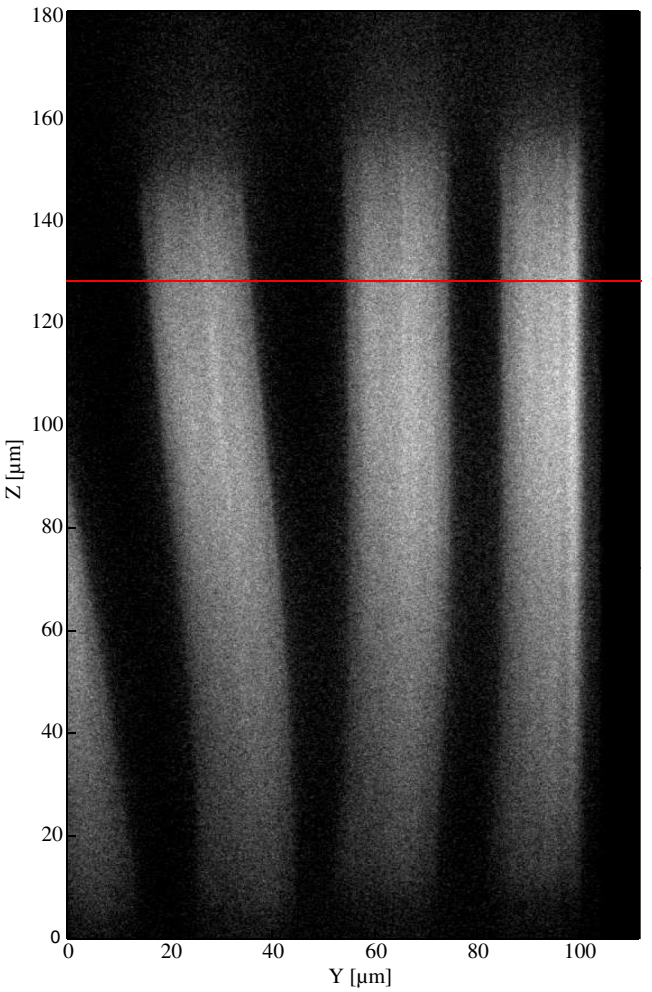

Fig. 5 Cross section of three pillars by CLSM. The line indicates the position of the cross section shown in Fig. 4. The silicon and glass interface are at the top and bottom of the figure, respectively.

A cross section along the height of the pillar is shown in Fig. 5. The pillar visible in the top left is bent at an angle of 5 deg and seems partially detached from the silicon interface. To the left is another pillar partially visible, showing the same problem.

This suggests that the sample tilt remaining after the tilt correction is approximately 0.04 deg, resulting in a slowly diminishing anchoring depth over the length of the rows and causing only partial anchoring in the last segment. The forces during the development phase, as discussed earlier, then cause bending or complete displacement of pillars if the adhesion at the glass is insufficient. In the most extreme cases pillars are removed altogether. This shows the importance of correct tilt and rotation correction for large-scale microstructures.

3.2.5 *Fabrication time*

The total fabrication time is long when compared to other rapid prototyping techniques, although those do not provide the same flexible 3-D fabrication capability. A possibility to speed up the process is to increase the line and plane separation, which was set to 400 nm and 2 μm, respectively. Considering the DLW focal spot size, the plane separation could have been increased to 4 μm, diminishing the writing time by almost 50%. Furthermore, a strategy can be employed where only the walls of the structure are written, trapping liquid resist inside that can be cured with an additional illumination step.[21]

3.3 *Acoustic mixing*

The confocal measurements were done at 10 μm from the glass channel interface, 100 ms integration time per frame, and 25 mW of laser power. The structure has a center-to-center pillar spacing Λ of 70 μm and is, in all other aspects, the same as the structure characterized in Sec. 3.2. The piezo excitation voltage is 16 V_{pp}.

The local acoustic field, composed of the fundamental channel resonance and the locally scattered fields, induces

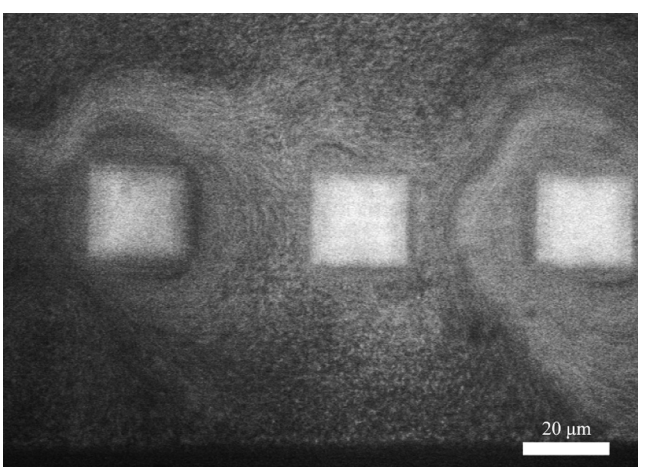

Fig. 6 Streaming induced flow around micropillars visualized by fluorescent tracer particles using CLSM. The external ultrasound is stopped after 18 s, causing the mixing to stop. The black line at the bottom is a measurement artifact, not the channel wall (Video 1, MPEG, 13.4 MB) [URL: http://dx.doi.org/10.1117/1.JM3.14.2.023503.1].

Rayleigh–Schlichting streaming at the pillar walls.[36,37] The streaming is visualized by fluorescent tracer particles around the pillars (see Fig. 6). The asymmetry of the streaming is likely to be caused by the slow bulk flow going to the right. The speed of the induced flow u_{ac} is approximately 30 μm s^{-1} and leads to rigorous mixing of the suspension in the vicinity of the pillars. To give an estimate of mixing performance, we assume a mixing flow around each pillar of u_{ac} and a flow distance required for mixing of $w_c/2$ (because of two rows). The structure would then require a mixing time of approximately $t = 6$ s. Since pillars over a length of $l = 12$ mm contribute to the mixing, this leads to an estimated flow rate of 7 μL min^{-1} which is comparable to other acoustic mixers[6,38,39] but not as fast as the fastest bubble mixer.[11]

4 Conclusion

We have demonstrated the fabrication of a 1.22-cm long micropillar micromixer using in-chip DLW. Most of the structure matches the designed double row very well. The largest source of deviation is caused by the motorized stage. Pillars that were consecutively written are accurately placed with micrometer precision. The fabricated pillars show good bonding with both the glass and silicon and are strong enough to withstand forces in the order of millinewtons.

The intrinsic fluorescence of the acrylic-based resist allows for straightforward optical characterization. Both fluorescence microscopy as well as CLSM was employed to successfully assess the fabricated structure.

We have demonstrated the proof-of-principle of a novel type of ultrasonic micromixer, based on locally inducing flows on micropillars embedded inside the microchannel. The local streaming flow speed in the vicinity of the pillars is 30 μm s^{-1}, which would yield an estimated flow rate of approximately 7 μL min^{-1} with homogeneous mixing. The fabrication technique explored is able to precisely fabricate a long mixing structure, which is important for high flow rate mixing. This combined with further research on the effect of pillar placement and 2-D/3-D shape on the induced streaming flow and mixing efficiency will likely lead to improvement of the micropillar-based micromixer, which combines robustness and stability with higher throughput flows.

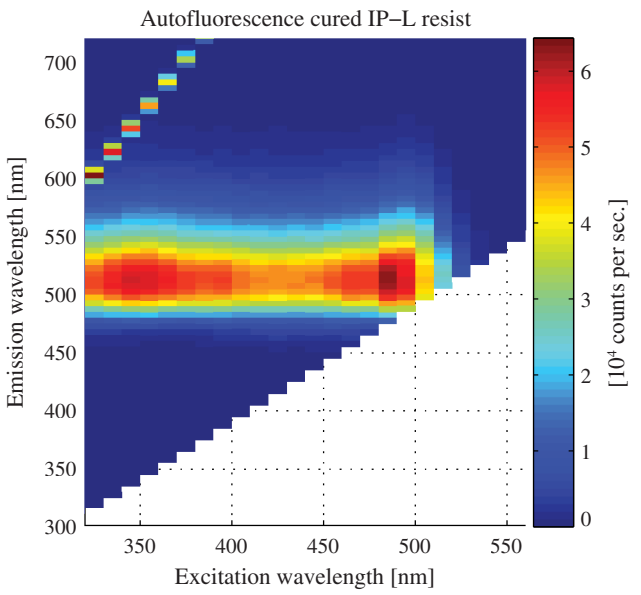

Fig. 7 Autofluorescence map of polymerized IP-L resist. A strong fluorescence emission band around 510 nm can be observed for excitation wavelengths from 520 nm down to 300 nm. The strong signal at emission wavelengths from 600 to 700 nm is a grating artifact.

Appendix: Autofluorescence Map of Cured IP-L

Using the autofluorescence of the polymerized resist only the structures are visualized, providing background-free 3-D imaging. Although the fluorescence is used to our advantage, in other experiments, the autofluorescence can be highly interfering (i.e., biofluorescence experiments). Therefore, it is useful to provide a fluorescence map of the developed resist as a reference for future work. The autofluorescence excitation-emission map of cured IP-L resist was measured (F900 fluorometer, Edinburgh Instruments) and is shown in Fig. 7.

Acknowledgments

The authors thank Daniel Wijnperlé for fabrication of the microchannels and Somnath Ghosh for assistance with the mixing experiments. This work is part of the research programme of the Foundation for Fundamental Research on Matter, which is part of the Netherlands Organisation for Scientific Research. This work was performed in the cooperation framework of Wetsus, center of excellence for sustainable water technology (www.wetsus.nl). Wetsus is funded by the Dutch Ministry of Economic Affairs. The authors would like to thank the participants of the research theme "sensoring" for the fruitful discussions and their financial support.

References

1. N.-T. Nguyen and Z. Wu, "Micromixers: a review," *J. Micromech. Microeng.* **15**(2), R1–R16 (2005).
2. V. Hessel, H. Lwe, and F. Schnfeld, "Micromixers: a review on passive and active mixing principles," *Chem. Eng. Sci.* **60**(8–9), 2479–2501 (2005).
3. C.-Y. Lee et al., "Microfluidic mixing: a review," *Int. J. Mol. Sci.* **12**(5), 3263–3287 (2011).
4. T. M. Squires and S. R. Quake, "Microfluidics: fluid physics at the nanoliter scale," *Rev. Mod. Phys.* **77**, 977–1026 (2005).
5. T.-D. Luong, V.-N. Phan, and N.-T. Nguyen, "High-throughput micromixers based on acoustic streaming induced by surface acoustic wave," *Microfluid. Nanofluid.* **10**(3), 619–625 (2011).
6. G. Yaralioglu et al., "Ultrasonic mixing in microfluidic channels using integrated transducers," *Anal. Chem.* **76**(13), 3694–3698 (2004).
7. P.-H. Huang et al., "An acoustofluidic micromixer based on oscillating sidewall sharp-edges," *Lab Chip* **13**(19), 3847–3852 (2013).
8. S. A. Elder, "Cavitation microstreaming," *J. Acoust. Soc. Am.* **31**, 54–64 (1959).
9. D. Ahmed et al., "A fast microfluidic mixer based on acoustically driven sidewall-trapped microbubbles," *Microfluid. Nanofluid.* **7**(5), 727–731 (2009).
10. A. Hashmi et al., "Oscillating bubbles: a versatile tool for lab on a chip applications," *Lab Chip* **12**, 4216–4227 (2012).
11. D. Ahmed et al., "A millisecond micromixer via single-bubble-based acoustic streaming," *Lab Chip* **9**, 2738–2741 (2009).
12. R. H. Liu et al., "Hybridization enhancement using cavitation microstreaming," *Anal. Chem.* **75**, 1911–1917 (2003).
13. R. H. Liu et al., "Bubble-induced acoustic micromixing," *Lab Chip* **2**, 151–157 (2002).
14. F. Serra et al., "Nematic liquid crystals embedded in cubic microlattices: memory effects and bistable pixels," *Adv. Funct. Mater.* **23**(32), 3990–3994 (2013).
15. M. H. Olsen et al., "In-chip fabrication of free-form 3D constructs for directed cell migration analysis," *Lab Chip* **13**, 4800–4809 (2013).
16. L. Amato et al., "Integrated three-dimensional filter separates nanoscale from microscale elements in a microfluidic chip," *Lab Chip* **12**, 1135–1142 (2012).

17. S. A. Vanapalli et al., "Microfluidic valves with integrated structured elastomeric membranes for reversible fluidic entrapment and in situ channel functionalization," *Lab Chip* **9**, 1461–1467 (2009).
18. Y. Liao et al., "Direct laser writing of sub-50 nm nanofluidic channels buried in glass for three-dimensional micro-nanofluidic integration," *Lab Chip* **13**, 1626–1631 (2013).
19. Y. He et al., "Overpass at the junction of a crossed microchannel: an enabler for 3D microfluidic chips," *Lab Chip* **12**, 3866–3869 (2012).
20. I. Izquierdo-Lorenzo, S. Jradi, and P.-M. Adam, "Direct laser writing of random au nanoparticle three-dimensional structures for highly reproducible micro-SERS measurements," *RSC Adv.* **4**, 4128–4133 (2014).
21. D. Wu et al., "Femtosecond laser rapid prototyping of nanoshells and suspending components towards microfluidic devices," *Lab Chip* **9**, 2391–2394 (2009).
22. G. M. Whitesides, "The origins and the future of microfluidics," *Nature* **442**, 368–373 (2006).
23. J. Wang et al., "Embellishment of microfluidic devices via femtosecond laser micronanofabrication for chip functionalization," *Lab Chip* **10**, 1993–1996 (2010).
24. S. Takayama et al., "Patterning cells and their environments using multiple laminar fluid flows in capillary networks," *Proc. Natl. Acad. Sci. U. S. A.* **96**, 5545–5548 (1999).
25. E. Delamarche, D. Juncker, and H. Schmid, "Microfluidics for processing surfaces and miniaturizing biological assays," *Adv. Mater.* **17**, 2911–2933 (2005).
26. M. Iosin et al., "Laser microstructuration of three-dimensional enzyme reactors in microfluidic channels," *Microfluid. Nanofluid.* **10**, 685–690 (2011).
27. D. Wu et al., "Three dimensional functional microfluidic chips fabricated by hybrid femtosecond laser microfabrication," in *2013 Conf. on Lasers and Electro-Optics Pacific Rim (CLEO-PR)*, pp. 1–2 (2013).
28. H. Bruus, "Acoustofluidics 7: the acoustic radiation force on small particles," *Lab Chip* **12**(6), 1014–1021 (2012).
29. W. M. Haynes, *CRC Handbook of Chemistry and Physics*, 95th ed., CRC Press 2014.
30. C. S. Miner, N. N. Dalton, and W. A. Hamor, Eds., *Glycerol: American Chemical Society Monograph Series*, Vol. 117, Literary Licensing, LLC, Montana (2013).
31. A. B. Richou, A. Ambari, and J. K. Naciri, "Drag force on a circular cylinder midway between two parallel plates at very low Reynolds numbers. Part 1: Poiseuille flow (numerical)," *Chem. Eng. Sci.* **59**, 3215–3222 (2004).
32. M. M. Zdravkovich, "Flow around circular cylinders," in *A Comprehensive Guide Through Flow Phenomena, Experiments, Applications, Mathematical Models, and Computer Simulations, Vol. 1, Fundamentals*, M. M. Zdravkovich, Ed., Oxford University Press, Oxford (1997).
33. B. Semin, J. P. Hulin, and H. Auradou, "Influence of flow confinement on the drag force on a static cylinder," *Phys. Fluids* **21**, 103604 (2009).
34. S. Sen, S. Mittal, and G. Biswas, "Flow past a square cylinder at low Reynolds numbers," *Int. J. Numer. Methods Fluids* **67**, 1160–1174 (2011).
35. S. C. Yen, K. C. San, and T. H. Chuang, "Interactions of tandem square cylinders at low Reynolds numbers," *Exp. Thermal Fluid Sci.* **32**, 927–938 (2008).
36. L. Rayleigh, "On the circulation of air observed in Kundt's tubes, and on some allied acoustical problems," *Philos. Trans. R. Soc. London* **175**, 1–21 (1884).
37. S. S. Sadhal, "Acoustofluidics 13: analysis of acoustic streaming by perturbation methods," *Lab Chip* **12**, 2292–2300 (2012).
38. T. Frommelt et al., "Microfluidic mixing via acoustically driven chaotic advection," *Phys. Rev. Lett.* **100**(3), 034502 (2008).
39. Z. Yang et al., "Ultrasonic micromixer for microfluidic systems," *Sens. Actuators A* **93**(3), 266–272 (2001).

Jorick van 't Oever is a PhD candidate at the University of Twente in Enschede. He received his MSc degree in applied physics from the University of Twente on the topic of dark plasmonic resonances in gold ring resonators in 2011. His research interests include (nonlinear) wave interactions, microfluidics, and interferometry.

Niels Spannenburg is a master's student at the University of Twente. He received his BSc degree in advanced technology from the University of Twente in 2013. His current research interests include thin film ceramic oxides and nanofabrication.

Herman Offerhaus obtained a PhD in solid-state laser technology in 1997. He spent two years at the ORC in Southampton to work on fiber lasers and nonlinear optics. This was followed by high-harmonic generation and electron spectroscopy/imaging at the AMOLF Institute in Amsterdam. At the University of Twente, he is a senior lecturer in the optical sciences group. He explores nonlinear vibrational spectroscopy and microscopy as well as plasmonics, nanooptics, and IR imaging.

Dirk van den Ende got his PhD in molecular physics at the Radboud University Nijmegen in 1982. After four years in industrial research, he joined the rheology (now physics of complex fluids) group at the University of Twente. His research focuses on the physical aspects of suspensions and their behavior in microchannels and on atomic force spectroscopy of thin electrolyte films on charged substrates. He (co-)authored nearly 100 peer-reviewed articles.

Jennifer Herek received her PhD in femtosecond spectroscopy from California Institute of Technology in 1996. After six years at Lund University as a postdoctoral researcher and assistant professor, she became group leader at the Biomolecular Control Group at AMOLF Institute. Subsequently, she became chair of the optical sciences group (2006) and dean of the Academy of Technology and Liberal Arts and Sciences (2012) at the University of Twente. She published over 120 peer-reviewed articles.

Frieder Mugele obtained his PhD at the University of Konstanz in 1997 on diffusion on metal surfaces in ultrahigh vacuum followed by research at Lawrence Berkeley Laboratory. At the University of Ulm, he extended his work to wetting of functionalized surfaces. Since 2004, he has been full professor of physics of complex fluids at the University of Twente. He has published more than 130 scientific articles including the >1000 times cited review on electrowetting.